International Research Journal of Engineering and Technology (IRJET) e-ISSN: 2395-0056
Volume: 09 Issue: 06 | June 2022 www.irjet.net p-ISSN: 2395-0072

Zero-Current-Switching Current-Fed Half-Bridge Isolated DC/DC Converter for Fuel-Cell Applications

Alekhya Patcha[1], Bharath Manduri[2], Sagar Malapati[3], Dr. Rama Devi Neerukonda[4], Nageswara Rao Nagarakanti[5]

Department of Electrical and Electronics Engineering,Bapatla Engineering College,Andhra Pradesh,India

---

Abstract - *This paper presents a dual inductor based current-fed bidirectional isolated snubberless dc/dc converter for fuel cell and photovoltaic inverters. This proposed converter provides a higher voltage conversion and zero switch turn-off voltage spike without snubber circuit. Most of the dc/dc converters require additional components and snubber for reduce voltage spikes. But in this paper, to eliminate the voltage spike problem by adding soft-switching features to the operated converters. Thus, the soft-switching technique avoids the need of snubber circuit, voltage across the switches is naturally clamped and voltage across switch is independent of the duty cycle. A formal mathematical design parameters are discussed for 300W converter.*

***Key Words*: Bidirectional Converter, dc/dc converter , fuel cells, renewable energy sources, soft-switching**

1. INTRODUCTION

In recent years the green energy and clean environment is attracted the attention of industries and common men. With the concept of smart system like smart grid, smart industries, alternative energy sources, smart transportation, hybrid micro-grid , and efficient smart power conversion is getting increasing importance day by day. Alternative energy sources (solar PV, Wind) cannot be used directly because the output is unregulated and low power output. Therefore, a power converter is needed to convert their output which is regulated and high-power output. Maximum power from alternative energy sources is extracted and supplied to dc grids and local loads. Mainly the converters are used in solar based electric vehicle charging station due to low power output of the solar PV systems. So, the boost converters are used in this applications to improve the fuel efficiency, utilization and the current ripple of the fuel cell stack must be minimized [1]. DC/DC conversion is very important in fuel cellor photo voltaic inverters. Several converter topology techniques have been reported [2]-[10].All the soft-switching converter techniques are studied and has justified current-fed half bridge topology is suitable for fuel cell applications [2]- [4]. In the year2004,the authors R.Gopinath et al.emphasison.

Active-clamping zero-voltage switching PWM current-fed half- bridge isolated dc/dc converter [11]. An active-clamp helps in achieving soft switching of devices and absorbs the turn-off voltage spike across the switches. An active clamp dissipates 1% of the output power.

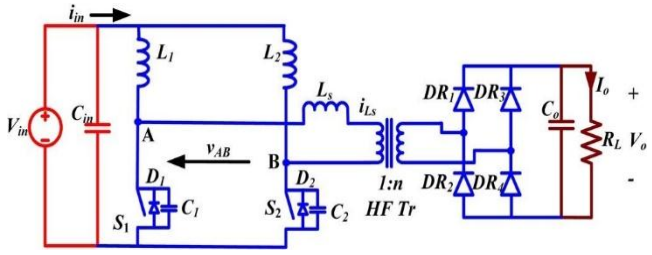

Fig-1: Conventional hard-switched current-fed half-bridge isolated dc/dc converter.

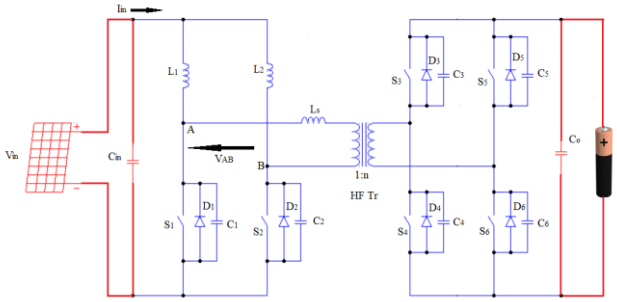

Fig-2: Proposed ZCS current-fed half-bridge dc/dc converter with full bridge on secondary.

A novel zero-current-switching current-fed half-bridge isolated dc/dc converter for fuel-cell based applications isproposed for improving performance of the power converter. The voltage across the switches is clamped without snubber circuit which makes the reduction in size, low cost, compactness and high efficiency. In the proposed converter, the commutation is done by natural commutation and switching transition losses are reduced and negligible circulating current. The soft-switching is better load efficiency than hard switching(Fig.1). The proposed converter as shown in Fig.2 can be used for fuel cells, electric vehicles and has a bi-directional ability. In this proposed converter the input is given from solar and output is stored in battery. This paper demonstrates converter operation and design of the converter and simulation results. The paper layout is as follows. Operation of the converter and analysis of the converter is explained in section 2. The detailed converter design is explained in

section 3. The proposed converter analysis and design are verified by simulation results using MAT LAB in section 4

2. OPERATION AND ANALYSIS

In this section , steady-state operation and analysis with ZCS high step-up dc/dc converter have been explained. The following assumptions are made for converter analysis:1)Boost inductors L1 and L2 are large enough to maintain constant current.2)Magnetizing inductance of the high frequency (HF) transformer is infinitely large.3)Ls is the series leakage inductance of the transformer, and all the components are ideal. The switches of primary side S1 and S2 are operated with gate signals which are phase shifted by 180°.The primary side duty cycle is denoted by D and secondary side duty cycle is denoted by d_s. Here, the primary side duty cycle is always greater than 50% and secondary side duty cycle is always less than 50%.

The converter operation during different intervals in a half cycle is explained using the equivalent circuits shown in Fig-3-10.

***Interval* a ($t_0<t<t_1$):**In the first interval, primary side switches S1 and S2 are conducted and sharing 50% each of the input current. Power is fed to the load by output capacitor and switch currents and inductor currents are half of the supply current i.eiL1=iL2=iS1=iS2=$I_{in}/2$.

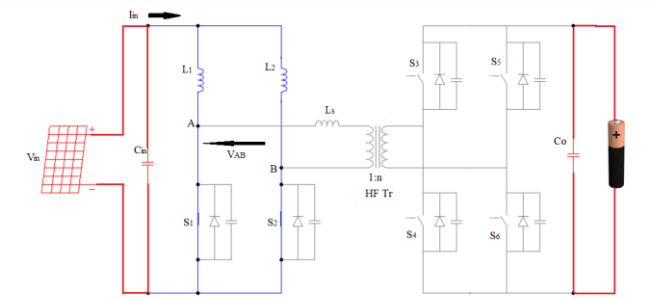

Fig-3

***Interval* b ($t_1<t<t_2$):** In this interval, secondary side switches S4 and S5 are turned on at $t=t_1$.It causes voltage V_o/n to appear across the primary of the transformer, and transformer leakage current iL_s starts building up. Hence, the inductor current iL_1,which was earlier flowing through switch S1,is diverted to the primary of the transformer. Therefore, current iS_1 through switch S1 starts decreasing linearly, and current iLs starts increasing .At the end of this interval, switch S1 current reduces zero, causing ZCS turn-off since the gating signal has not been removed yet.

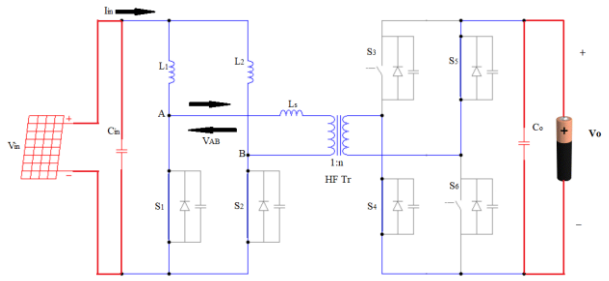

Fig.4

***Interval* c ($t_2<t<t_3$):**In this interval, diode D1 of the switch S1 starts conducting at $t=t_2$. The currents through the transformer and the switches S2, S4,and S5 are increasing with the same slope. At the end of this interval currents i_{Ls} and iS_2 reach their peak value. The peak value depends upon the pulsewidth of the gating signal applied to secondary switches.

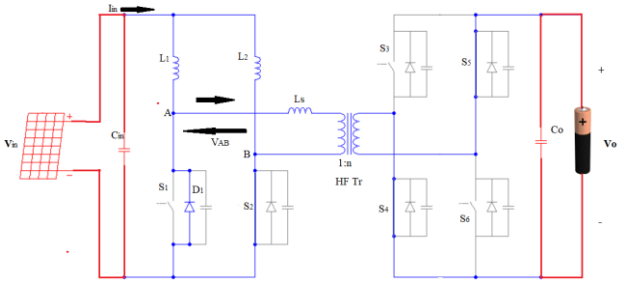

Fig.5

***Interval* d ($t_3<t<t_4$):**In this interval, secondary side switches S4 and S5 are turned off at $t=t_3$.The current on the secondary side is taken over by diodes D3 and D6 across secondary switches S3 and S6.

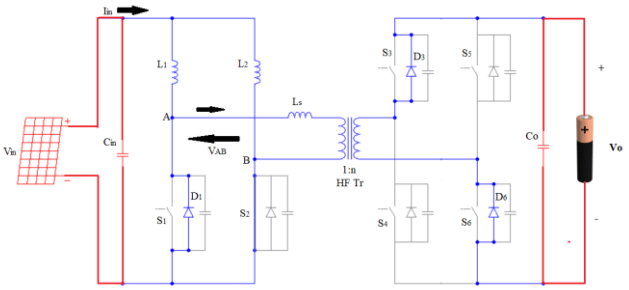

Fig.6

***Interval* e ($t_4<t<t_5$):** In this interval, the snubber capacitor across the primary switch S1 charges to voltage Vo/n.

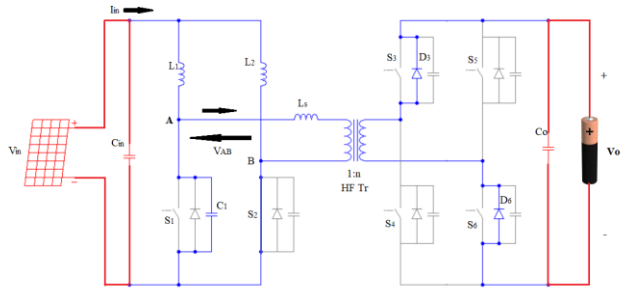

Fig.7

***Interval* f (t_5<t<t_6):** In this interval, the transformer primary voltage is zero. Therefore, a constant current $I_{in}/2$ flows through its primary. switch S2 conducts full input current I_{in}. Output capacitor C_0 is charged by constant current $I_{in}/2n$ through the diodes D3 and D6.

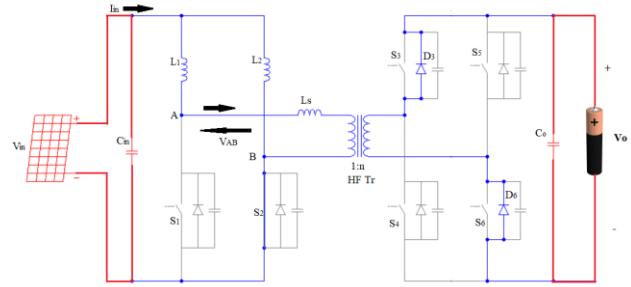

Fig.8

***Interval* g (t_6<t<t_7):** During this interval, at t=t_6,primary switch S1 is turned on. The snubber capacitor across it discharges through the series snubber resistance, and switch voltage reduces to zero at the end of this interval.

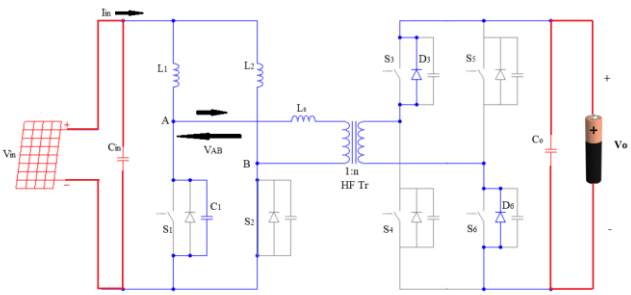

Fig.9

***Interval* h (t_7<t<t_8):** In this interval, a negative voltage -Vo/n appears across the transformer primary, and its primary current starts falling from $I_{in}/2$.switch S1 current starts increasing, current iLs is transferred to switch S1. This is the zero-current turn-on of switch S1.at the end of this interval at t=t_8,current iL_s reduces to zero, and switch current iS1 increases to $I_{in}/2$.

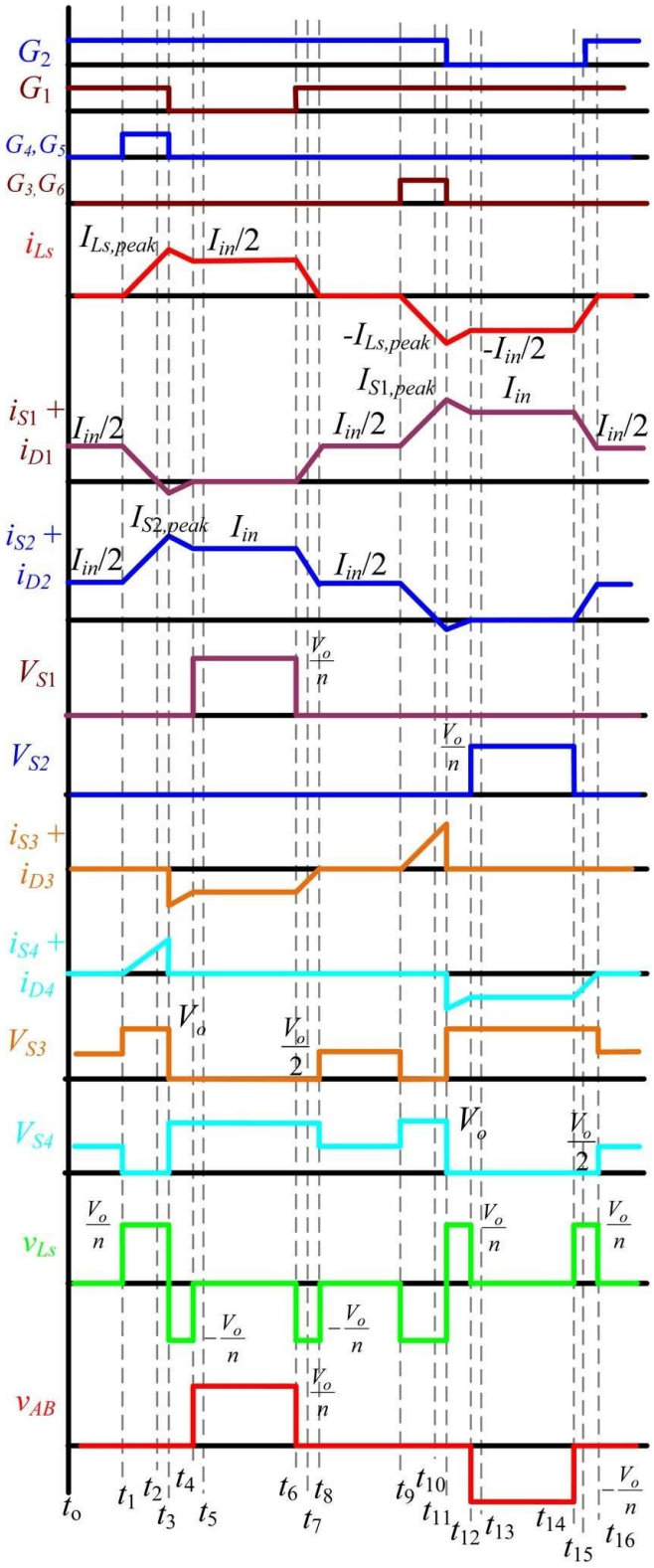

Fig-11: Operating waveforms of proposed ZCS two-inductor current-fed half-bridge isolated dc/dc converter

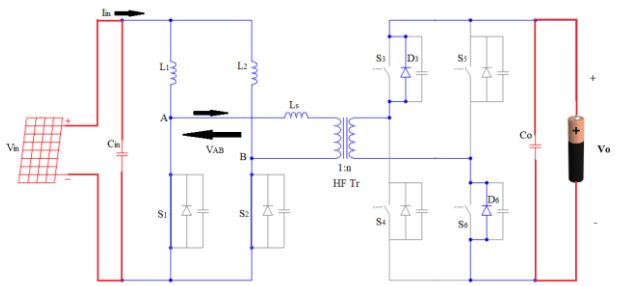

Fig.10

For next half cycle, the intervals are repeated in a similar sequence with other symmetrical devices conducting to complete the full cycle.

3. DESIGN OF THE CONVERTER

In this section, the procedure for converter design is explained by a design example for the following specifications chosen for fuel cell inverter application: input voltage Vin = 24V, Output voltage V_0 = 350V,Output power P_0 = 300W, and switching frequency fs = 100KHZ.

1) The average input current is

$$I_{in} = P_0/(\eta V_{in}).$$

Assuming an ideal efficiency η of 100%,I_{in}= 12.5A.

2) The maximum voltage across the primary switches is

$$V_{sw} = \frac{V_0}{n} \quad (1)$$

3) Input and output voltages are related as

$$V_0 = \frac{n \cdot V_{in}}{(1-D)} . \quad (2)$$

4) Series inductance Ls is calculated using

$$L_s = \frac{2 \cdot V_0 \cdot d_s}{n \cdot I_{in} \cdot f_s} . \quad (3)$$

5) The rms current through the primary switches is given by

$$I_{sw,rms} = I_{in}\sqrt{\frac{9+4d_s-6D}{12}} . \quad (4)$$

6) High-frequency transformer design: The transformer turn ratio is selected to gain low conduction losses in primary switches. The efficiency of the converter depends upon losses in primary switches due to conduction of high current.

In HF transformer the losses are copper losses and core losses. The selection of transformer with high turns ratio requires lower voltage rating switches [using(1)] and low ON-state resistance this requirement leads lower conduction loss. The leakage inductance of the transformer Ls decreases with the increase of turns ratio, thus improving the power transferring capability of the converter. Power transferring ability is limited by the leakage inductance of the HF transformer. In this regard, when the converter works in the reverse direction regenerative braking is happen and absorbs the energy ,smaller leakage inductance will result in smaller duty cycle loss. However, higher turns ratio yields higher switch RMS current [from (2) and (4)].The switches are selected based on the emerging maximum voltage required for the EV chargers. The maximum value of duty ratio corresponding to an input voltage of 24V is calculated using equation (2) for different values of transformer turn ratio and keeping the secondary duty ratio d_s to 0.05.Using corresponding ON-state resistance the conduction losses in primary switches are determined.

The primary turns and secondary turns of the transformer is determined for various turn ratios, for all cases keep the maximum flux density in core identical. Gauge winding is selected based on primary winding and secondary currents, and winding resistances are calculated.

Here, low-cost devices of similar values are selected based on voltage rating. Here, d_s is set to 0.05. Using equation (3), the leakage inductance of transformer is determined to be Ls = 6.22μH. The peak voltage across the secondary switches is equal to output voltage V_0.Peak and rms values of the transformer primary current are

$$I_{Ls,peak} = \frac{V_0 \cdot d_s}{n \cdot f_s \cdot L_s} \quad (5)$$

$$I_{Ls,rms} = I_{in}\sqrt{\left[\frac{(1-D)}{2} + \frac{d_s}{3}\right]} \quad (6)$$

7) The necessary condition of ZCS of primary switches is

$$d_s \geq \frac{I_{in} \cdot n \cdot L_s \cdot f_s}{2 \cdot V_0} \quad (7)$$

For ensuring ZCS, the value of d_s is kept a little higher than the critical value given by equation (7). For this additional time, the antiparallel diode of the switch conducts. However, in order to limit the circulating and peak current through the components, d_s should not be higher than the critical value.

8) Boost inductors: The boost inductor values are given by

$$L_1 = L_2 = (V_{in})(D) / [(\Delta I_{in})(f_s)] \quad (8)$$

Where ΔI_{in} is the boost inductor ripple current.

For ΔI_{in} = 1A, L = 176μH.

9) Secondary switches: The peak current through the secondary switches is

$$I_{sw,sec,Peak} = \frac{I_{in}}{2 \cdot n} \quad (9)$$

10) Output capacitor: The value of output filter capacitor C_0 is

$$C_0 = \frac{(I_0) \cdot (D - 0.5)}{\Delta V_0 \cdot f_s} \quad (10)$$

Where ΔV_0 is the allowable ripple in output voltage and C_0 = 4.2 μF for ΔV_0 = 0.5V. Its voltage rating is equal to V_0 = 350V.

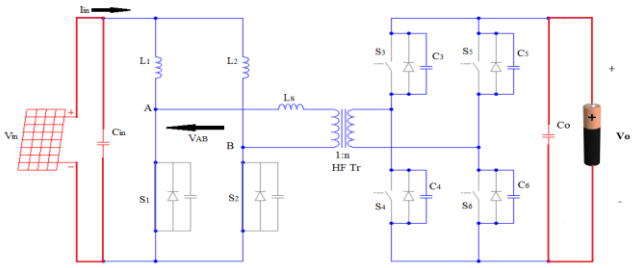

Fig-12:Equivalent circuit during intervals a and h

4. EFFECT OF DEVICE PARASITIC

In section 2 steady-state analysis of the converter is explained. The devices used in practical converter system have parasitic. Due to output capacitance the performance of the converter does not change, it slightly transforms the operating waveforms during a few intervals.

The effect of the output capacitance of the secondary switches is prominent in intervals a and h. At the end of interval h the transformer secondary current reduces to zero. The equivalent circuit during this interval is as shown in Fig.12. The resonant frequency is given by

$$\omega_s = \frac{1}{\sqrt{n^2 \cdot L_s \cdot C_{eq}}} \quad (11)$$

Where, C_{eq} is the equivalent capacitance across the secondary side transformer. Considering all device capacitances to be equal.

$$C_{eq} = C_3 = C_4 = C_5 = C_6 \quad (12)$$

During interval a the voltage across the switch capacitances are given by

$$V_{s3} = V_{s_6} = \frac{V_0}{2} + \frac{V_0}{2} cos[\omega_s (t - t_8)] \quad (13)$$

$$V_{s4} = V_{s5} = \frac{V_0}{2} - \frac{V_0}{2} cos[\omega_s (t - t_8)] \quad (14)$$

Currents through the primary of the transformer i_{Ls} and secondary i_{sec} are given

$$i_{sec} = -\frac{V_0}{\omega_s \cdot n^2 \cdot L_s} sin[\omega_s (t - t_8)] \quad (15)$$

$$i_{Ls} = -\frac{V_0}{\omega_s \cdot n \cdot L_s} sin[\omega_s (t - t_8)] \quad (16)$$

5. SIMULATION AND EXPERIMENTAL RESULT

In this section, simulation results for a 300W,100KHZ converter design are presented. For this converter Gate pulses G1,G2,G3,G4,G5,G6are triggered for the switches S1,S2,S3,S4,S5,S6 respectively. Simulation was performed on MATLAB to verify the analysis and design of the converter.

Table-5

In below table the output voltage, current and power are calculated theoretically for different turns ratios for constant capacitor rating.

Output voltage and current variations for different n values

Turns ratio (n)	*Capacitor rating*	*Voltage*	*Current*	*Power*
2.5	*4.6μF*	*317*	*0.93*	*294.81*
3.5	*4.6μF*	*325*	*0.91*	*295.75*
4	*4.6μF*	*350*	*0.858*	*300.05*
5	*4.6μF*	*340*	*0.86*	*292.4*
6	*4.6μF*	*347*	*0.84*	*291.48*

From the above table, concluded that for different turns ratios output voltage and current are varies but output power is approximately constant. At turns ratio 4 the output voltage is high as compared with other turns ratios. From the aforementioned discussion, designs with n=4 and 4.5 are competitive. However, with low switch rms current, i.e., low losses and better duty cycle range for voltage regulation over wide fuel cell voltage range, n=4 is selected for this application.

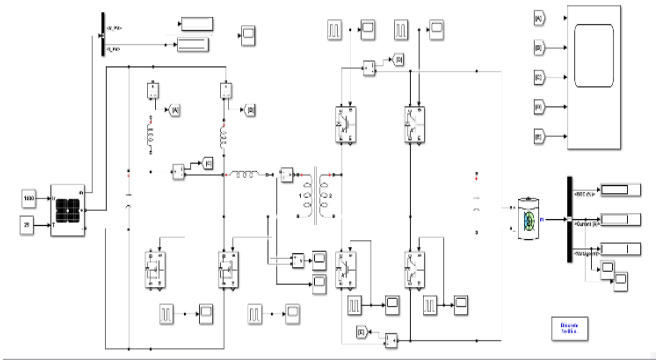

Fig-13: Simulation circuit

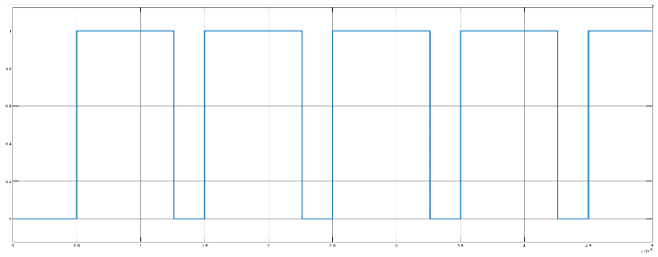

Fig-14: gate pulse (G1)

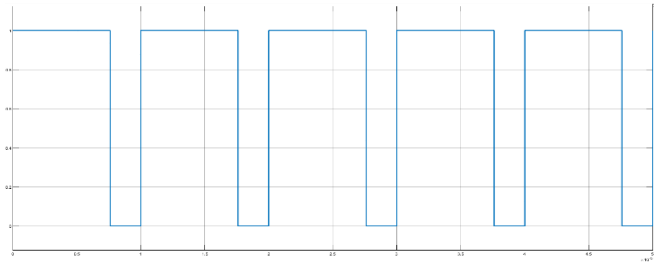

Fig-15: gate pulse (G2)

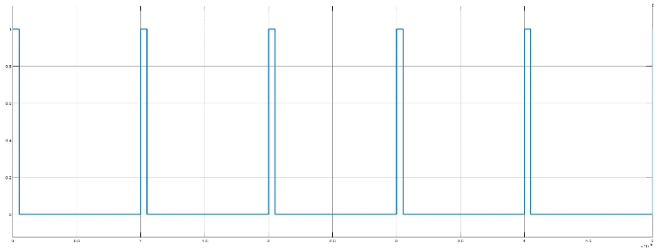

Fig-16: gate pulse (G3)

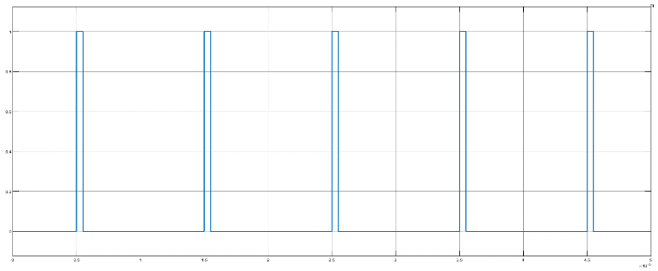

Fig-17: gate pulse (G4)

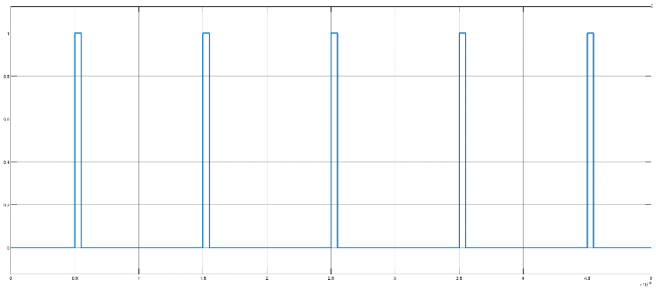

Fig-18: gate pulse (G5)

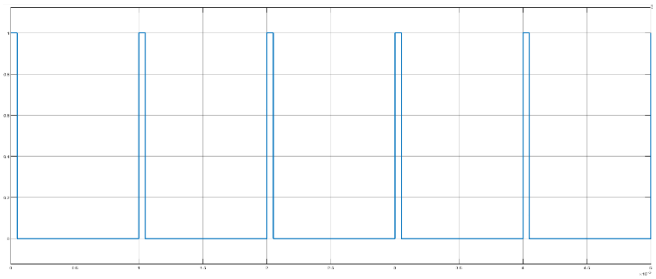

Fig-19: gate pulse (G6)

Fig-20 illustrates ZCS turn-off of the primary switches. The results clearly show that each switch current reaches zero naturally and the antiparallel body diode conducts, causing a zero voltage across the switch. Therefore, a switch turn-off snubber is not needed. In addition, the currents through the switches build up with a slope resulting in their zero-current turn-on.

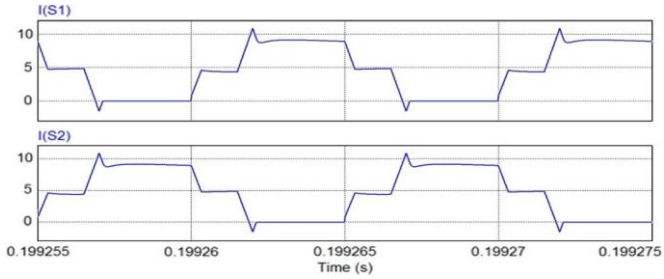

Fig.20. Current in the primary-side switches showing ZCS turn-off.

Fig-21 describes the current through the secondary switches, including the current through their body diodes. The results show the zero-current turn-on of secondary switches as the current starts conducting from zero and builds up with a slope that depends upon the reflected value of Ls. Voltage becomes zero when either the diode conducts or the switch is turned on. When switches S4 and S5 are conducting, the voltage across switch S3 is Vo. Voltages across all the switches become Vo/2, when current through the antiparallel diode reaches zero. Fig-22 also shows the voltage across the primary of the transformer. Whenever one of the primary switches is turned off, output voltage is

reflected across the primary of the transformer. Voltage VAB is zero during conduction of both the primary switch.

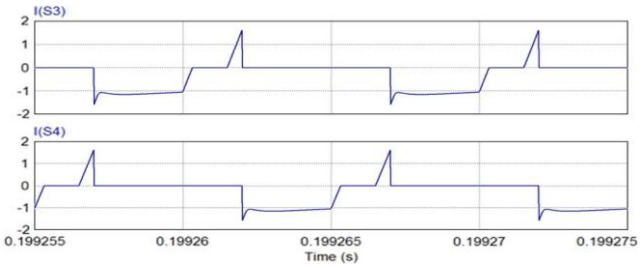

Fig-21: Current flowing through the secondary Side switches.

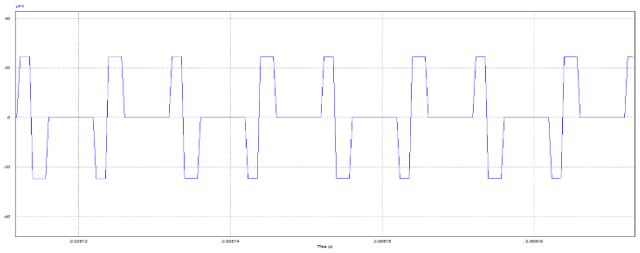

Fig-22: Voltage across the primary of the transformer

Fig.23 shows the transformer primary current. The simulation waveform of current iLs matches with that of the analysis performed in Section II. The ripple frequency of iL1 and iL2 is the same as switching frequency fs = 100 kHz. Since these two currents are phase shifted by 180◦ , the ripple frequency of input current Iin is 200 kHz, which is twice the switching frequency fs.

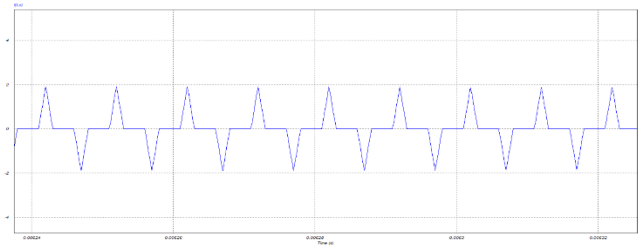

Fig-23: Current across the primary of the transformer

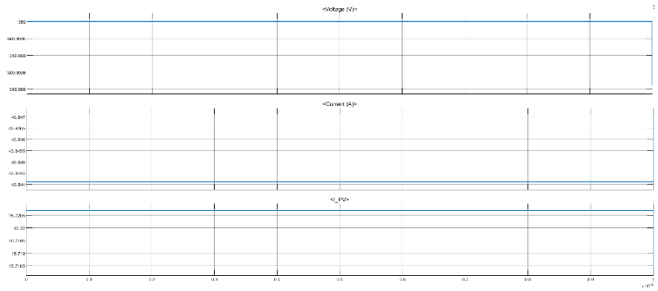

Fig-24: Output voltage, output current and input current waveforms

6. SUMMARY AND CONCLUSION

This paper has proposed a novel current-fed converter that provides a secondary-side-modulation-based solution which eliminates switch turn-off voltage spike problem. Because of this relieves the need of extra snubber circuit, making the proposed concept novel and snubber less. This reduces component count and peak current through the primary switches, and size of the transformer has been reduced. Voltage of the primary-side switches is clamped at reflected output voltage. Therefore, a design with selection of low-voltage devices is possible. Low-voltage and low-current devices are less costly and result in compact converters. In addition, such devices have low ON-state resistance, resulting in low conduction losses, and enhance converter efficiency and maintains soft switching of all the devices as well as natural or zero-current commutation of body diodes of primary devices as well as secondary diodes, resulting in low switching losses. Steady-state operation, analysis, and design of the proposed converter have been presented effectively and proposed converter has bidirectional power flow ability. Thus, this converter topology is suitable for low-voltage high-current applications such as fuel cell, PV, and battery source applications.

REFERENCES

[1] S. K. Mazumder, R. K. Burra, and K. Acharya, “A ripple-mitigating and energy-efficient fuel cell power-conditioning system,” IEEE Trans. Power Electron., vol. 22, no. 4, pp. 1437–1452, Jul. 2007.

[2] S. Han, H. Yoon, G. Moon, M. Youn, Y. Kim, and K. Lee, “A new active-clamping zero-voltage switching PWM current-fed half-bridge converter,” IEEE Trans. Power Electron., vol. 20, no. 6, pp. 1271–1279, Nov. 2005.

[3] S. J. Jang, C. Y. Won, B. K. Lee, and J. Hur, “Fuel cell generation system with a new active clamping current-fed half-bridge converter,” IEEE Trans. Energy Convers., vol. 22, no. 2, pp. 332–340, Jun. 2007.

[4] A. K. Rathore, A. K. S. Bhat, and R. Oruganti, “Wide range ZVS active-clamped L–L type current-fed DC–DC converter for fuel cells to utility interface: Analysis, design and experimental results,” in Proc. IEEE Energy Convers. Congr. Expo., 2009, pp. 1153–1160.

[5] J. Mazumdar, I. Batarseh, N. Kutkut, and O. Demirci, “High frequency low cost DC–AC inverter design with fuel cell source home applications,” in Conf. Rec. IEEE IAS Annu. Meeting, 2002, pp. 789–794.

[6] Y. J. Song, S. K. Chung, and P. Enjeti, “A current-fed HF link direct DC/AC converter with active harmonic filter for fuel cell power systems,” in Conf. Rec. IEEE IAS Annu. Meeting, 2004, pp. 123–128.

[7] J. Wang, F. Z. Peng, J. Anderson, A. Joseph, and R. Buffenbarger, "Low cost fuel cell converter system for residential power generation," IEEE Trans. Power Electron., vol. 19, no. 5, pp. 1315–1322, Sep. 2004.

[8] R. Gopinath, S. Kim, J-H. Hahn, P. N. Enjeti, M. B. Yeary, and J. W. Howze, "Development of a low cost fuel cell inverter system with DSP control," IEEE Trans. Power Electron., vol. 19, no. 5, pp. 1256–1262, Sep. 2004.

[9] M. H. Todorovic, L. Palma, and P. Enjeti, "Design of a wide input range DC–DC converter with a robust power control scheme suitable for fuel cell power conversion," in Proc. IEEE APEC, 2004, pp. 374–379.

[10] M. J. Khan, M. T. Iqbal, and J. E. Quaicoe, "Utility interactive fuel cell inverter for distributed generation: Design considerations and experimental results," in Proc. IEEE Can. Conf. Elect. Comput. Eng., 2005, pp. 583–586.